Mechanisms of the imbibition behavior in shales: A critical review

Cite as: AIP Advances 13, 080701 (2023); doi: 10.1063/5.0161989
Submitted: 13 June 2023 • Accepted: 10 July 2023 •
Published Online: 7 August 2023

Mingcan Wang,[1,2] Weijun Shen,[1,2,a)] Tianran Ma,[3] Zhi Zeng,[1,2] and Fengchang Yang[4]

AFFILIATIONS

[1] Key Laboratory for Mechanics in Fluid Solid Coupling Systems, Institute of Mechanics, Chinese Academy of Sciences, Beijing 100190, China
[2] School of Engineering Science, University of Chinese Academy of Sciences, Beijing 100049, China
[3] School of Mechanics and Civil Engineering, China University of Mining and Technology, Xuzhou, Jiangsu 221116, China
[4] State Key Laboratory of Nonlinear Mechanics, Institute of Mechanics, Chinese Academy of Sciences, Beijing 100190, China

[a)] **Author to whom correspondence should be addressed:** wjshen763@imech.ac.cn

ABSTRACT

Despite the success of hydraulic fracturing in yielding large production increases from shale gas reservoirs, uncertainties associated with basic transport processes require understanding in order to improve the efficiency and minimize environmental impacts. The hydraulic fracturing process brings in large volumes of water into shale reservoir formations, most of which remains unrecoverable and interferes with shale gas production. The imbibition behavior in shales is commonly observed during the hydraulic fracturing process, and the mechanism greatly influences the hydrocarbon recovery in shale gas reservoirs. In this review, the imbibition models in shales are briefly summarized using the Lucas–Washburn model, piston repulsion model, capillary bundle model, and scalar model. Then the experimental study and numerical simulation of shale imbibition are discussed. Moreover, the influencing factors of the imbibition behavior in shales are analyzed, such as shale and fluid properties. Finally, the main conclusions and the future research direction prospects of the imbibition behavior in shale gas reservoirs are summarized. An accurate description of the imbibition behavior in shale is crucial for optimizing the hydraulic fracturing design and enhancing shale gas production in the development of shale gas reservoirs. It is proposed that the research on the individual influencing factors of shale percolation and the geological mechanism under coupling should be strengthened and that the research on the experimental aspects of shale powder percolation should be emphasized.

I. INTRODUCTION

Shale gas has become one of the important supply sources for satisfying the oil and gas energy demand in the United States and Canada, and its related extraction technology is becoming more mature. According to statistics, the shale gas reserves in China are close to 25 trillion cubic meters, mainly located in the Sichuan Basin, Ordos, the Tarim Basin, and other regions.[1,2] China's gas-bearing shale formations are characterized by high thermal maturity and a high degree of later modifiability. Shale gas reservoirs are also mainly characterized by terrestrial deposits with a complex distribution. Organic shale gas will become one of the important sources of fossil energy in China in the future.[3] Shale gas targets with potential for extraction have been detected and realized in southwestern China.[4] Shale gas extraction requires the use of high-pressure surface pumps to create fractures by pushing highly viscous fracturing fluid through the wellbore into the reservoir. When the pressure exceeds the fracture pressure of the reservoir rock near the bottom of the well, the rock will be pressed open and fractured.[5]

After the fracturing process, the residual fracturing fluid and the rock will undergo complex seepage, so understanding the seepage characteristics of shale is an important guide to shale gas extraction.[6,7] Shale seepage is an important manifestation of the interaction between the fracturing fluid and shale. Seepage is a common phenomenon in conventional porous media, but due to the complex pore structure and non-uniform nature of shale, the mechanism of shale seepage is relatively incomplete. Lucas and Washburn proposed that the seepage distance in capillaries is time-dependent,[8,9] but the Lucas–Washburn (LW) model has not been sufficiently applicable.[10] In recent years, with the lucubrate study

of shale seepage, many scholars have proposed modified equations based on this model to cope with more complex seepage situations. In the experimental study of seepage, the mainstream research method is to use the nuclear magnetic resonance (NMR) technique to investigate the seepage mechanism. Combined with simulation techniques such as molecular dynamics and the lattice Boltzmann method, the seepage process can be more accurately obtained.[9,11,12]

In this review, the imbibition models in shales are summarized using four models, namely, the LW model, piston repulsion model, capillary bundle model, and scalar model. Then the experimental study and numerical simulation of shale imbibition are discussed. Moreover, the influencing factors of the imbibition behavior in shales are analyzed. Finally, the main conclusions and the future research directions prospects of the imbibition behavior in shale gas reservoirs are summarized.

II. IMBIBITION MODELS IN SHALES

Although the term "seepage" has been predominantly used for petroleum since 1994, studies on seepage began early and have led to the development of a more comprehensive theory of seepage. The earliest seepage models are the Lucas–Washburn (LW) equation and the Handy model,[9,13] which simplify the seepage process by treating the shale interior as a capillary system. They researched the seepage process within a single capillary to obtain the relationship between seepage distance and time, but they ignored the influence of inertial forces and so on. Thus, there exist the problem of low applicability. On this basis, many scholars have proposed a relatively accurate but complex extended seepage model, which can more accurately describe the spontaneous water absorption process in different wettability capillaries. Under different rock boundary conditions, the related descriptions such as OEO (one end open) and TEO (two end open) have been proposed.[14]

A. Lucas-Washburn model

As early as 1918, Richard used percolation experiments with liquids of different viscosities on absorbent paper to study the relationship between the amount of liquid percolation and time in the capillary system. Then he proposed a percolation capillary system based on the fact that different solutes have different rates of diffusion behavior on paper.[8] Washburn proposed a dynamic theory on liquid percolation in capillaries in 1921,[9] which simplified the problem to a single capillary, as shown in Fig. 1. However, the initial advancing distance of the liquid at the A end l_0 and the air resistance were ignored. The final percolation distance vs time was given as

$$l^2 = \frac{\left(P_A + D \cdot g \cdot h + \frac{2\gamma}{r}\cos\theta\right)\left(r^2 + 4\varepsilon r\right)t}{4\eta}, \tag{1}$$

where r is the radius of the circular tube section, h is the liquid depth, P_A is the external driving pressure, η is the liquid viscosity, D is the liquid density, γ is the surface tension of the liquid, θ is the contact angle, and ε is the sliding coefficient.

It can be seen that the percolation distance of the liquid in the capillary is proportional to $\sqrt{t}$.

Based on the simplification ideas provided by the above-mentioned model, many scholars have conducted extended studies

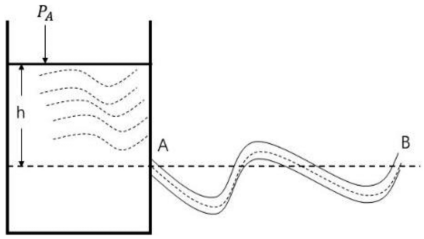

FIG. 1. Schematic diagram of the percolation model.

to give a modified form of the LW equation. Wang *et al.* established a circular cross-sectional tilted composite capillary model composed of capillary walls with different wettabilities to study the modified LW equation for capillary wettability[15] and then solved the model numerically to find what large effect the capillary wall component content, capillary radius, and oil–water viscosity ratio have on the spontaneous oil–water swelling process. Free energy is related to the area and slope under the swelling profile, and it was found that the volume-based wettability evaluation criterion underestimated the degree of hydrophobicity of the studied rock samples.[7] For the analytical calculation of the LW equation, Hamraoui and Nylander identified that the driving force of liquid permeation in capillaries was the interfacial pressure difference,[16] which ignored the effect of inertial forces and considered only gravity and surface tension, and expressed the other effects using retardation coefficients β_1, giving an analytical calculation of the LW equation. Combining the LW equation with the Laplace pressure yields

$$h(t) = \frac{1}{4\eta}\left[-r\beta_1 + \sqrt{r^2\beta_1^2 + 8\eta\left(r\beta_1 h(0) + 2\eta h^2(0) + r\gamma\cos(\theta_0)t\right)}\right], \tag{2}$$

where β_1 is the retardation factor, γ is the surface tension of the liquid, r is the capillary radius, θ is the contact angle, ρ is the density of the liquid, and h is the equilibrium height within the capillary.

This equation yields h proportional to $\sqrt{t}$, which is consistent with the results of the Washburn equation. The effect of gas type, formation depth, organic acid concentration, carbon number, and silica nanofluid on SI kinetics was studied and evaluated using the modified LW equation.[4] The SI rate was found to increase with gas generation, and the following equation is given:

$$L = \sqrt{4\left(\frac{k}{R_{PT}}\right)\left(\frac{\gamma_{LG}}{\mu}\right)\cos\theta_A t}, \tag{3}$$

where L is the distance of the brine spontaneous imbibition (at time t), k is the rock permeability, μ is the brine viscosity, R_{PT} is the average pore throat radius, γ_{LG} is the liquid–gas interfacial tension, and θ_A is the advancing brine contact angle of the rock–brine–gas system.

B. Piston repulsion model

Handy found that the gas phase is discontinuous during the percolation,[13] and for regions where the gas is not flowing, the

pressure gradient of the capillary is not able to provide a flowing pressure gradient. It results in the following hypothesis: water undergoes piston-like displacement in the capillary, and the pressure gradient at the front edge of the suction front is negligible. Combining the Darcy equation, the capillary pressure equation, and the continuity equation yields the following equation:

$$Q_w^2 = \left(\frac{2P_c k_w \phi A^2 S_w}{\mu_w}\right) t, \tag{4}$$

where A is the cross-sectional area of the capillary, ϕ is the partial porosity, s_w is the pore water content, k_w is the effective permeability, μ_w is the water viscosity, and P_c is the capillary pressure.

The model put forward by Handy does not consider the change in relative permeability and the effect of gravity, making the square of the increase in percolation vs the time curve of swelling not cross the origin of the coordinates, and the percolation of the porous medium is infinite at infinity, which is obviously wrong. Li and Horne proposed an expression for the amount of percolation, considering capillary force and gravity for this problem,[10] and found out how to calculate the effective water permeability k_W and capillary pressure P_c using the following equation:

$$P_c = \frac{1}{(S_{wf} - S_{wi})} \frac{a}{b} \Delta\rho g L, \tag{5}$$

$$k_W = \frac{\mu_W}{A\Delta\rho g} b, \tag{6}$$

where $a = \frac{Ak_w(S_{wf}-S_{wi})}{\mu_w L} P_c$, $b = \frac{Ak_w}{\mu_w}\Delta\rho g$, and S_{wf} is the water saturation.

The expression for the rate of water absorption Q_W is also given,

$$Q_w = \frac{dN_{wt}}{dt} = a\frac{1}{R} b, \tag{7}$$

where R is the absorption recovery expressed in terms of pore volume and N_{wt} is the volume of water absorbed by the core.

The Handy model is widely used, but its assumptions are simpler and less accurate. It also has some limitations such as not considering the flow relationships between capillaries. In a single capillary channel, percolation is driven by a single interface, while in a porous medium, it is driven by the leading edge of the wetted phase formed by the interaction of multiple interfaces. Percolation in capillary channels is usually divided into two models. One is a model of percolation with one end closed and one end open, called the OEO model. The other is with both ends open, called the TEO model, as shown in Fig. 2. Standnes researched samples with different shapes and boundary conditions to investigate the effects of co-flow and counter-flow seepage on oil recovery,[14] and he also proposed a classification method for the above-mentioned models.

Fischer researched the spontaneous absorption and swelling of cylindrical Berea sandstone cores by simulating OEO conditions through tectonic experiments[17] and gave an expression for the position of the front end of the liquid surface during the percolation

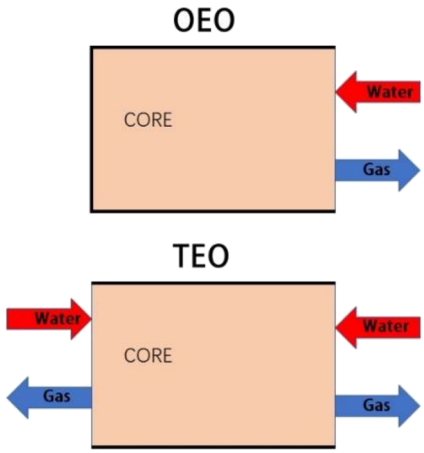

FIG. 2. Schematic diagram of physical models of OEO and TEO.

process x. The expression for the position of the front end of the liquid surface during percolation is given as

$$x^2 = \frac{2(P_{cf} - P_{cb})}{\frac{\mu_0}{A_0 k_{A0}} + \frac{\mu_W}{A_W k_{AW}}} \frac{t}{R\phi A}, \tag{8}$$

where P_{cf} is the effective capillary pressure at the leading edge of the suction, P_{cb} is the capillary pressure at the opening, A_0 is the cross-sectional area of the oil-bearing region, A_W is the cross-sectional area of the water-phase region, μ_0 is the viscosity of the oil-phase, k_{A0} is the associated permeability of the region, k_{AW} is the associated permeability of the water-phase, R is the oil recovery, ϕ is the rock porosity, A is the cross-sectional area of the core, and t is the percolation time.

Mathematical analysis was used to correct the viscosity term, and the mathematical expression of the TEO model was proposed.[12,18] The authors concluded that when the fluid viscosity ratio changes, the effective relative permeability used for standard analysis changes significantly and the final oil production is proportional to the square root of time.

C. Capillary bundle model

The shale interior is porous and has a complex pore structure. The capillary bundle model simplifies the shale interior into closely spaced capillary bundles for study, as shown in Fig. 3. When oil and gas are displaced by water, they pass through the large capillaries, and then the more viscous liquids are replaced by less viscous liquids so that the shape of the recovery curve depends on the size and number of capillaries.[5,19] A capillary beam rheometer based on the capillary beam model principle is used to perform adhesion measurements of low velocity Newtonian fluids.[20] The adhesion force is shown in Fig. 4, and F_W is given using the following equation:

$$F_W = \rho g \Delta h - \frac{8L\eta Q_m}{n\rho\pi R^4}, \tag{9}$$

where ρ is the fluid density, g is the gravitational acceleration, n is the number of capillary tubes, Q_m is the mass flow rate, η is the fluid

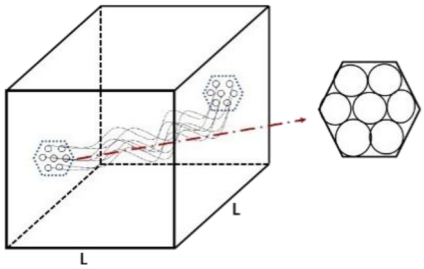

FIG. 3. Physical model of the capillary bundle.

viscosity, and Δh is the difference between the inlet and outlet fluid levels.

Combining the capillary bundle model with other theories to study different shale percolations is the main utilization direction of this model at present. Cai and Yu combined the capillary bundle model with fractal theory to establish a fractal model for the seepage coefficient of oil and gas reservoirs[21] and derived the analytical equation of seepage volume vs time as follows:

$$V_{Wt}^2 = (A\varphi)^2 \frac{\sigma \cos\theta}{4\mu} \frac{D_f \lambda_{\max}}{1 - D_f} \left[\left(\frac{\lambda_{\min}}{\lambda_{\max}} \right)^{D_f} - \frac{\lambda_{\min}}{\lambda_{\max}} \right] t. \quad (10)$$

It can be seen that the percolation volume is linearly related to the square root of time. The flow rate through the capillary bundle Q is expressed as the sum of the flow rates of the individual capillary,[5] which gives the expression for the permeability of the capillary bundle model,

$$k = \frac{\mu L N}{A \Delta P} \int_{\lambda_{\min}}^{\lambda_{\max}} q(\lambda) f(\lambda) d\lambda, \quad (11)$$

where A is the cross-sectional area of the porous medium, L is the linear length of the porous medium, ΔP is the pressure difference between the two ends, $\lambda_{\max}$ and $\lambda_{\min}$ are the maximum and minimum diameters of the capillary, respectively, $q(\lambda)$ is the flow function, $f(\lambda)$ is the probability density distribution function, and N is the total number of capillaries.

When calculating the permeability as a function of stress field, Sun *et al.* combined the capillary bundle model with the volume strain to give the percolation flow equation for a single capillary bulk phase fluid.[22] The value of the capillary bundle can be calculated as a composite of several single capillaries,

$$q = \frac{\pi r^4}{8\mu L} \Delta P - \frac{\pi r^4 |\ln r - 0.5|}{\mu} \varepsilon - \frac{2\pi r^3}{3\mu} \tau_0, \quad (12)$$

where r is the capillary radius, L is the capillary length, μ is the fluid viscosity, ΔP is the pressure difference between the two ends of the capillary, ε is the interfacial action coefficient, and τ_0 is the fluid yield stress.

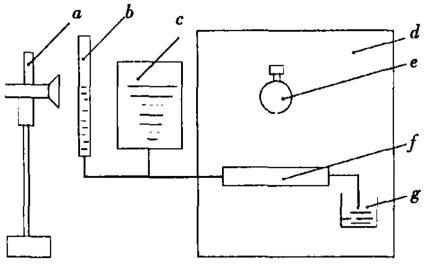

FIG. 4. Schematic diagram of the capillary bundle rheometer.

D. Scaling model

The effect of these factors on the seepage process can be studied qualitatively by introducing the scalar equation.[23] In the study of the nature of linear water drive, the rate of oil repulsion is considered to depend on the length of the capillary and the rate of water injection, which gives the following equation of complete repulsion considering the capillary pressure:

$$f \frac{\partial s}{\partial t} + V \frac{dF}{ds} \frac{\partial s}{\partial x} - \frac{k}{c\mu_w} \frac{\partial}{\partial x} \left[K_0 F \frac{dP_c}{ds} \frac{\partial s}{\partial x} \right] = 0, \quad (13)$$

where V is the injection rate, c is the oil–water viscosity ratio, F is the permeability to viscosity ratio, s is the water saturation, μ_w is the water viscosity, K_0 is the relative permeability of water, and P_c is the capillary pressure.

The scaling equation was used to calculate the rate of oil recovery by spontaneous seepage.[24] The result was expressed as a relationship between the rate of oil recovery and the causeless time to obtain a more generalized scaling equation for a strong water-wet system, and the causeless time t_D was expressed as

$$t_D = \left[\frac{1}{L_C^2} \frac{\sigma}{\sqrt{\mu_o \mu_W}} \sqrt{\frac{K}{\phi}} \right] t. \quad (14)$$

In a subsequent study, Ma *et al.* considered wettability as a key factor in determining the capillary driving force and the associated percolation rate, and they proposed a new method to quantify wettability from the percolation rate.[24] The wettability index relative to the percolation work is defined by plotting the pseudo-percolation capillary pressure curve, as shown in Fig. 5. It gives pseudo-self-absorption capillary pressure vs water content saturation, which expresses the dimensionless time as

$$t_D = \left[\frac{1}{L_C^2} \frac{\sigma}{\mu_m} \sqrt{\frac{K}{\phi}} \right] t. \quad (15)$$

For the calculation of the dimensionless time, different relations are established for the cases of water and gas parallel flow, t_d, self-priming counter-current, t_D, and relative permeability with time, t_{NEW},[10,18,25]

$$t_d = c^2 \frac{k_w}{\phi} \frac{P_c^*}{\mu_w} \frac{S_{wf} - S_{wi}}{L_a^2} t, \quad (16)$$

$$t_D = \frac{2}{L_C^2} \sqrt{\frac{K}{\phi}} \frac{\sigma t}{\mu_w \left(1 + \sqrt{\mu_{nw}/\mu_w} \right)}, \quad (17)$$

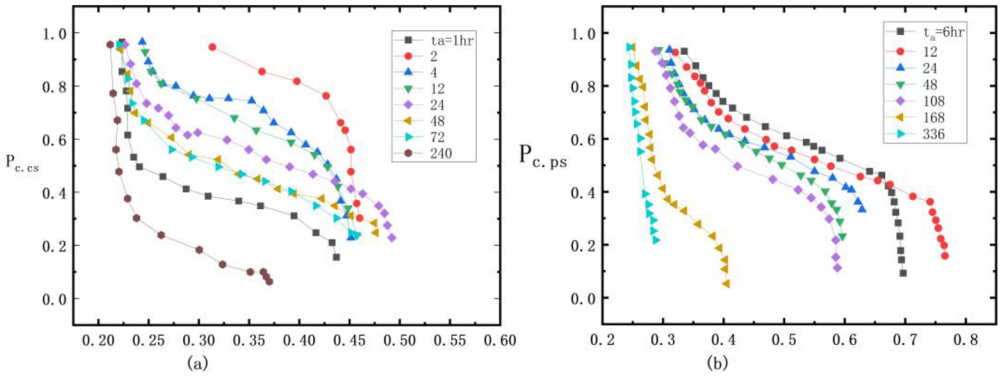

FIG. 5. Capillary pressure vs water saturation.

$$t_{NEW} = \frac{\mu_2}{\mu_1 - \mu_2}\left[\sqrt{1 + \frac{\sqrt{\frac{2k}{\phi}\sigma(\mu_1 - \mu_2)t}}{\mu_2^2 L_C^2}} - 1\right]. \tag{18}$$

III. EXPERIMENTAL RESEARCH OF SHALE IMBIBITION

The current seepage experiment is the main method to research the shale seepage phenomenon, and the method is relatively easy to implement and can visually observe the changes in the experimental core. However, there are some disadvantages, such as it is difficult to simulate the pressure, temperature, and other conditions in the real shale reservoir. The main research methods for seepage experiments include nuclear magnetic resonance (NMR),[26,27] the volumetric method,[28,29] the mass method,[30–32] and CT imaging.[33–35] The volumetric method and mass method combined with NMR are the mainstream experimental methods at present.

A. Overview of osmosis

The percolation phenomenon refers to the entry of a liquid into the interior of a porous medium by capillary action on the contact surface without an additional pressure difference. The diffusion of ink on paper, the absorption of water by soil, and the absorption of dye by fabric all include the phenomenon of percolation. The porosity of shale is low; most of the pore diameters are at the nanometer level, which has strong capillary force, and liquids can easily enter the shale under the action of capillary force. Conformal percolation means that the direction of water inhalation and oil outflow is the same,[10] that is, the direction of the inhalation phase and discharge phase is the same, generally occurring at the late stage of hydrophilic bottom percolation. Reverse percolation refers to the opposite direction of water and oil flow, where the direction of the inhaled phase and the direction of the expelled phase are opposite, which generally occurs in low-permeability reservoirs when the resistance of oil and water through the pore space is higher and oil seeps out from around the core.[36]

The Bond number N_B^{-1} is generally used as a criterion when determining the type of percolation,[37] which was proposed by Schechter and defined as

$$N_B^{-1} = C\sigma\sqrt{10^{11} \times \frac{\emptyset}{K}}/(\Delta\rho g H), \tag{19}$$

where C is the constant, σ is the interfacial tension, ϕ is the porosity, K is the permeability, and H is the porous media height. When N_B^{-1} is greater than 1, it is mainly reverse osmosis; when N_B^{-1} is less than 1, and it is mainly *cis*-percolation.

Li and Horne made a correction and gave the following formula:[25]

$$N_B^{-1} = 2C\sigma\cos\theta\sqrt{10^{11} \times \frac{\emptyset}{K}}/(\Delta\rho g H), \tag{20}$$

When N_B^{-1} is greater than 5, reverse osmosis occurs; when N_B^{-1} is between 0.2 and 5, *cis*-osmosis and reverse osmosis occur together; when N_B^{-1} less than 0.2, *cis*-osmosis occurs.[25]

B. Nuclear magnetic resonance technique

NMR was discovered in 1946, and the NMR technology has become a powerful tool for studying the seepage phenomenon. By scanning shale cores with NMR instruments, it is possible to monitor the distribution of oil and gas being displaced and the fluid between pores, which makes it a reliable method to study shale seepage.

Meng *et al.* found through NMR that liquids preferentially fill small pores during saturated percolation in the Longmaxi Formation shale and vice versa for unsaturated absorption.[38] The saturated seepage of liquids in typical shale formations in the Sichuan Basin, Ordos Basin, and Qaidam Basin was studied comparatively using NMR.[26] It was found that microfractures in marine shales gradually extend during water absorption while matrix pores in terrestrial shales are compacted or destroyed, leading to pore blockage and consequently to a decrease in T_2 values. The cores were scanned and analyzed by the NMR technique, the saturation of flowable fluid can be obtained using centrifugal and gas drive methods,[26] and the void size distribution of the rock can be obtained in combination with gas adsorption experiments.[39,40] Sun *et al.* used the NMR technique to obtain the saturated and dry spectra of shale cores from the Shahezi Formation in the Songliao Basin.[41] The results in Fig. 6 show that the core is dominated by nanoscale inorganic pores and the T_2

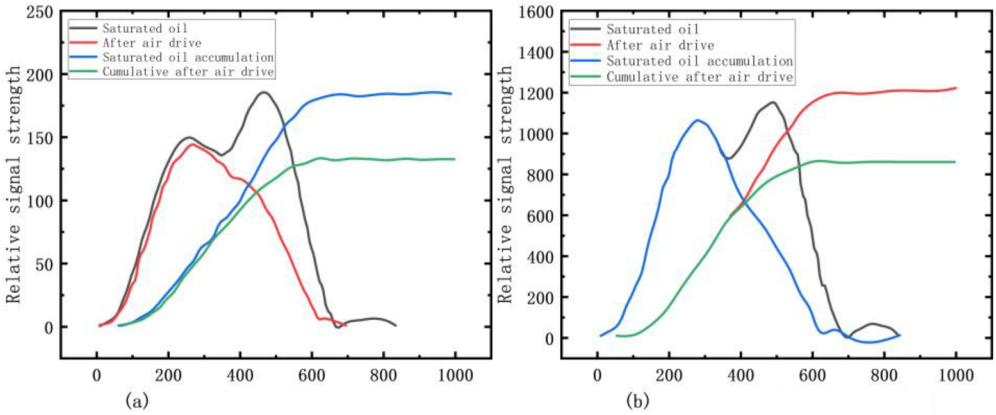

FIG. 6. NMR spectra of 2 shale cores from well A6 before and after gas drive.

spectrum is dominated by single peaks with relatively undeveloped microfractures.

Although NMR techniques are widely used in shale percolation experiments, there are problems such as the influence of paramagnetic minerals on the detection signal and the small test pore size due to bound fluids. The application of the NMR technique is focused on full-scale characterization of pore distribution, porosity measurement, analysis of percolation fluid flow and type, and wettability discrimination.[42] Sun *et al.* proposed that the effect of influencing substances (clay water, bitumen, pyrite, etc.) and the results should be determined and corrected by combining numerical simulation techniques.[41] They also pointed out that the influence on the shale NMR T_2 spectrum should be calculated by changing the surface relaxation rate of clay water, asphalt, pyrite, etc. In the future, unsupervised learning methods can also be combined to analyze the position of the $T_1 - T_2$ 2D spectrum of free hydrocarbons and the saturation of free oil.

C. Volume method and mass method

The volumetric method refers to an experimental method for measuring the volume of oil coming out of a percolation drive. The oil emergence pattern of the core is researched by reading the scale change of the suction meter or capillary metering tube. The volumetric method was used to study the effect of various factors on spontaneous seepage in fractured low-permeability cores.[10] The effects of core length, oil–water viscosity ratio, matrix wettability, matrix water saturation, and different pressures on percolation in low-permeability sand and gravels were considered by a homemade experimental setup.[28] Other scholars researched the seepage mechanism and oil yield variation in different shale samples.[29,43,44] The adsorption processes of carbon dioxide and methane in Jilin Huadian shale samples were researched by gas adsorption experiments;[31] both were found to go through a rapid adsorption period first and then an adsorption equilibrium period, and the total amount of absorption increased with the increase in temperature and pressure. The VB language was used to solve the problems of inaccurate calculation of the gas compression factor and large error at high pressure in the volumetric method, which is given in Fig. 7.[45]

The mass method is used to research the percolation process by measuring the weight change of the sample. Since there is a displacement effect when percolation occurs, it will lead to a change in sample weight, and the percolation pattern can be investigated by recording the weight change. Yue *et al.* studied the isothermal adsorption and desorption of shale by the MSB magnetic levitation balance weight method.[46] Before the experiment, the shale cores need to be pretreated to exclude the effect of moisture and other gases on the adsorption experiment.

Different oil and gas substitutes can be selected when using the mass method for percolation measurements. The shale samples were soaked and dried using toluene, petroleum ether, and ethanol, after which the core basal signals were obtained using NMR instruments.[27] By completely drying the mud shale sample of the Ulalik Formation, followed by adding saturated n-dodecane in vacuum, the mass difference before and after is the feed oil mass.[32] Yang *et al.* investigated the mechanism of high-temperature thermally excited seepage increase in the outcrop shale of the Longmaxi Formation in the Sichuan Basin.[47] The experiments compared the different percolation effects of dry shale and water-bearing shale after high-temperature thermal excitation, and they found that the change in the rock mineral fraction and the increase in the micro-nano-pore throat led to the increase in percolation in dry shale and that the hydrated swelling of clay minerals and the proliferation of micro-fractures led to the increase in percolation in water-bearing shale. The effects of shale type and liquid immersion

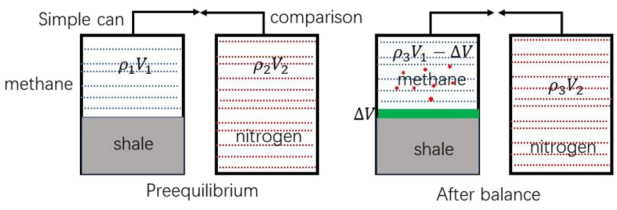

FIG. 7. Schematic diagram of the volumetric method considering the volume of the adsorbed phase.

on proppant embedding were investigated.[48] The results showed that the higher the clay content, the greater the self-absorption, and the proppant embedding depth is elevated after shale hydration.

D. CT imaging

With the development of optical technology, the microstructure of shale can be directly observed by using instrumental imaging, including 2D imaging techniques such as HIM and SEM and 3D imaging techniques such as FIB, micro-nano-CT, and micro-CT. CT imaging originated in the 1960s and 1970s, which scanned the sample by x-ray beams and obtained digital reconstruction images after processing, with the advantages of high accuracy. It is widely used in medical, geological, and other research fields.

The cracks, fractures, and rock skeleton in rock samples can be visualized by CT imaging. Shi *et al.* investigated the mechanism of hydrated fracture development in mud shale from three sections of the Sujiahe Formation in the western Sichuan area.[33] The imaging results showed that the brittle shale has a relatively significant capillary effect. Han *et al.* conducted micro- and nano-CT scanning experiments on dense reservoir cores in the Long 7 section of the Ordos Basin to realize the three-dimensional imaging display of the pore-throat system and found that the connectivity of the large throat channels in some shale cores is marvelous.[49] Qualitative characterization of the microscopic pore structure of the shale at this site has demonstrated that the shale oil in the Long 7 section has the geological basis for large-scale extraction.[35] Chen *et al.* systematically scanned the pore structure characteristics of marine shale using pore CT imaging technology in the Sichuan Basin and found that there were two types of shale fractures,[34] namely, microfracture and grain margin fracture. The pore types can be divided into organic pore, clay mineral intergranular pore, and mineral dissolution pore. The stress sensitivity of artificial fractures was investigated by CT scanning of shale cores from the Longmaxi Formation in the south Sichuan area before and after perimeter pressure and variable flow pressure tests, and it was found that the constant perimeter pressure and variable flow pressure tests were more consistent with the production reality.[50] Mao *et al.* reviewed the application of CT in detection of a rock's internal structure and elaborated the principle and progress of CT through *in situ* scanning experiments.[51] Using the DVC method combined with micro-CT or other 3D image techniques, together with *in situ* loading scanning devices, the internal deformation field of rocks can be effectively measured.

IV. NUMERICAL SIMULATION OF SHALE IMBIBITION

At present, in addition to experimental methods to study shale percolation phenomena, techniques such as numerical simulations can also be resorted. Numerical simulation methods have been widely adopted since the 1950s, and with the increase in computing power, numerical simulation has become a reliable method to complement experimental studies. Shale percolation simulation techniques require a description of the basic physical properties of the shale matrix and the shale fluid percolation. The main numerical simulation methods currently available are molecular dynamics methods, lattice Boltzmann methods, and finite element methods.

A. Molecular dynamics (MD) method

Molecular dynamics (MD) is a technique for studying fluid flow and its interaction with the flow medium at the molecular and submolecular scale. The MD method refers to the simulation of the process using a computer and involves a simple mechanism, namely, the conservation of the total energy (potential energy and kinetic energy) and the force acting on a fluid particle is usually a vector sum of the three components of the force arising from the interaction of the particle with other fluid particles, the force between the particle and the particles forming the solid wall, and the external force (gravity and pressure gradient) so that the force $\vec{F}$ on particle i can be written as

$$\overrightarrow{F(r_i)} = m_i a_i(t) = m_i \frac{d\vec{r}_i^{\,2}}{dt^2}, \tag{21}$$

$$m_i \frac{d\vec{r}_i^{\,2}}{dt^2} = F_1 + F_2 + F_3, \tag{22}$$

where F_1 is the force resulting from the interaction between the fluid particle i and the other fluid particles in the medium, F_2 is the force between the fluid particle i and the solid wall particles, F_3 denotes an external force, such as gravity, pressure gradient, etc., m_i is the mass of particle i, and $a_i(t)$ is the acceleration of particle i.

The transient flow pattern of oil in nanopores and the diffusion of decane on the graphene surface were investigated by using the constructed single-walled carbon nanotubes combined with MD.[11] Figure 8 shows that the percolation uptake in the carbon nanotubes increases linearly in a short time as the liquid filling rate increases significantly and as the tube becomes smaller due to the low time scale and the low friction on the inner wall of the graphite tube. After the simulation to study the density distribution and molecular structure of decane during the percolation process, it was found that the swelling rate decreased with the increase in the carbon nanotube radius.[52] The transport of oil through inorganic nanopores and the static properties and pressure-driven flow behavior of liquid hydrocarbons in inorganic nanopores of shale were studied and simulated by using the MD method.[53–55] Figure 9 shows that octane molecules with pore diameters below 1.8 nm diffuse slowly while the density, self-diffusion coefficient, and viscosity of octane molecules with pore

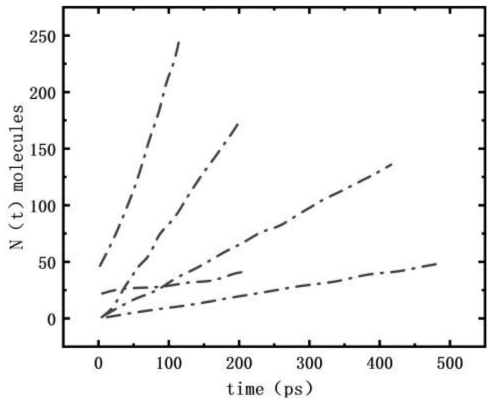

FIG. 8. Oil flow pattern in carbon nanotubes.

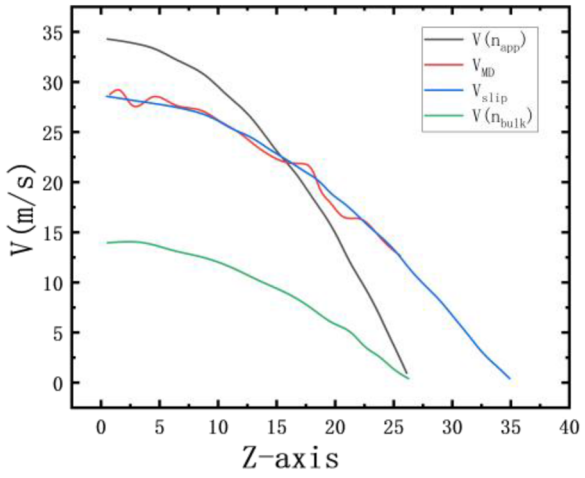

FIG. 9. Octane diffusion rate.

diameters larger than 3.6 nm tend to be equal to those of the continuum liquid.[11] Hong *et al.* combined molecular dynamics simulation and the pore network to research the gas transport properties and molecular mechanism in the pore network of non-homogeneous shale and obtained the gas transport velocity profile.[56] Hu *et al.* proposed a method to characterize the fluid diffusion mechanism in shale micro- and nano-pores.[57] They used a four-layer graphite slit structure to characterize the shale pore walls and obtained the velocity profiles and density distributions of methane molecules in nanopores under different pore sizes, temperatures, and pressure conditions by molecular dynamics simulations. The modified surface diffusion coefficients D_{sa} and Knudsen diffusion coefficients D_{km} are given as

$$D_{sa} = 6.5840 \times 10^{-7} T^{0.5} e^{-\frac{\Delta H^{0.8}}{RT}}, \tag{23}$$

$$D_{km} = B\frac{J_{km} RT}{M \nabla P}. \tag{24}$$

B. Lattice Boltzmann method

The LBM was developed in the 1980s to simulate the motion of fluids. Using the lattice Boltzmann equation is computationally efficient, and it can handle fluid systems consisting of an arbitrary number of mass and transport coefficient components. Linking the microscopic and macroscopic aspects, solving the fluid equations of motion with discrete models, simplifying complex boundaries, and combined with computational fluid dynamics software, it has a wide range of applications. The method simulates the fluid flow by solving a discretization of the kinetic Boltzmann equation defined on a finite lattice. The equation is simplified as[58]

$$f_i(t + \Delta t, r + v_i \Delta t) - f_i(t, r) = \frac{\Delta t}{\tau}\left[f_i^{(0)}(t, r) - f_i(t, r)\right]. \tag{25}$$

Due to its simplicity and versatility, the application of the LBM in complex and multi-scale flows is rapidly developing, most widely in entropic and turbulent, multiphase flows and deformable particle and fiber suspensions; interpolation rebound and immersion boundary-type methods are also very reliable in dealing with flows in nano- and micro-fluidic devices.[59] A multiphase multicomponent flow is simulated by using the LBM.[60] By introducing an interparticle potential, the model allows for massively parallel calculations by means of local calculations to simulate single-component flows with Reynolds numbers up to 10. Some scholars then simulated non-ideal gas and liquid phase transitions, focusing on the modeling of single-component fluid systems that follow the non-ideal gas equation of state, and obtained the overall density of the liquid and gas phases as a function of the class temperature parameter.[60]

Direct pore-scale simulations to understand the percolation behavior and its effects are often limited by the complexity of the pore geometry in the shale matrix and the problem of mixed wettability. To figure out this problem, an improved pseudopotential LBM was proposed to research the secondary seepage behavior of complex shale 3D porous structures in pore-scale simulations,[61] and the equilibrium density distribution function $f_\alpha^{\mathrm{eq}}(\mathbf{x}, t)$ is calculated by the following equation:

$$f_\alpha^{\mathrm{eq}}(\mathbf{x}, t) = w_\alpha \rho(\mathbf{x}, t)\left[1 + 3\frac{\mathbf{e}_\alpha \cdot \mathbf{u}^{\mathrm{eq}}}{c^2} + 4.5\frac{(\mathbf{e}_\alpha \cdot \mathbf{u}^{\mathrm{eq}})^2}{c^4} - 1.5\frac{(\mathbf{u}^{\mathrm{eq}})^2}{c^2}\right], \tag{26}$$

where $f_\alpha^{\mathrm{eq}}(\mathbf{x}, t)$ is the density distribution function in the direction of α, $w_\alpha = 1/3$ (α = 0), $w_\alpha = 1/18$ (α = 1–6), $w_\alpha = 1/36$ (α = 7–18), ρ is the macroscopic fluid density, $\mathbf{e}_\alpha$ denotes the velocity in 19 directions, and c is the velocity of the lattice.

Since the traditional continuity equation is no longer applicable due to the spatial boundary slip and non-homogeneity of viscosity and density due to the intermolecular interactions at the nanoscale, Wang *et al.* proposed a modified LBM to study liquid flow in nanoporous media.[62] This study used coupled molecular dynamics simulations and theoretical models to simulate the liquid flow in nanoporous media by the local visible viscosity LBM, which gives the following local apparent viscosity calculation equation:

$$\nu_{app}(\mathbf{x}) = \frac{1}{N}\sum_{\alpha=0}^{N} \frac{R_\alpha(\mathbf{x})\nu_{\alpha-eff}(\mathbf{x})\nu_{wall}}{R_\alpha(\mathbf{x})\nu_{wall} + 4\nu_{\alpha-eff}(\mathbf{x})l_s}, \tag{27}$$

where N is the number of velocity directions.

The authors extended the single pore flow to nanoporous media flow, which provided an idea for the extension of single pore to multiple pores. The results showed the velocity distribution of the LBM compared with that of the theoretical model. Jiao *et al.* used the LBM of heat flow simulation combined with the theory of rock damage development and developed a coupled pore-scale THM, which can calculate the THM information of fluid and the effect of fracture and rock damage on fluid conductivity.[63] Zhou *et al.* proposed a multi-scale model, as shown in Fig. 10.[64] The model combines molecular simulation with the LBM, where the local adsorption density parameter integrates and scales up the molecular simulation results into the LBM model to study the gas flow pattern in shale nanopores.

C. CFD and FEM methods

Computational fluid dynamics (CFD) is essentially a numerical simulation technique that uses discrete point variables to simulate

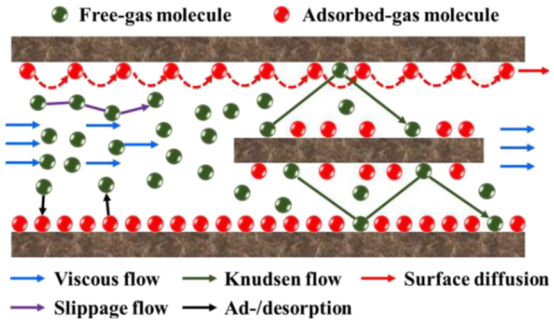

FIG. 10. Schematic diagram of gas molecule flow in shale microporosity.

continuous physical fields (temperature, velocity, pressure, etc.) in time and space and obtains an approximation of the variable fields by establishing and solving a system of fluid dynamics equations. The finite element method (FEM), also known as the matrix approximation method, is based on the basic principle of decomposing the solution domain into smaller subdomains and deriving the solution for the entire solution domain by approximating the solution for the subdomains.

Currently, CFD and the FEM can be combined with existing computational software for secondary development and applied to different research situations. The average flow velocity of the downward-sloping pipe is higher than that of the upward-sloping pipe, and the effect of the well slope angle on the water holding rate in stratified flow is more obvious, as shown in Fig. 11.[65] Samuel and Andrea used CFD numerical simulation combined with specific control equations and simulated flow in porous shale gas to investigate the diffusion behavior during seepage and the effect of fracture geometry on flow and found that the early flow behavior of shale is determined by the geometry of fractures.[66]

The use of fracturing technology for the transformation of shale formations can significantly improve the production of shale reservoirs, and it can significantly improve the research efficiency. A numerical model of proppant flow and transport in the horizontal wellbore based on CFD was established to study the proppant

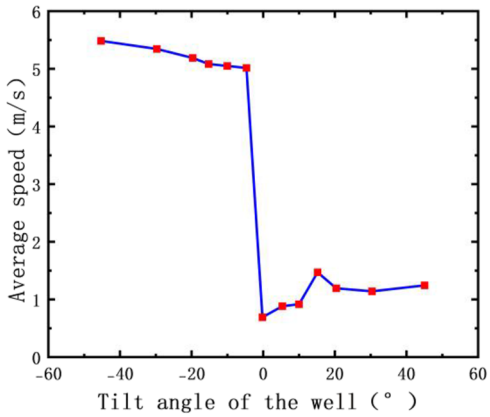

FIG. 11. Relationship between the well slope angle and average flow rate.

transport law in deep shale horizontal fractured wellbores.[67] The reservoir hydraulic-mechanical coupled FEM was established, and the AFI fracturing process was numerically simulated using the continuous medium method.[68] The process of hydraulic fracturing in naturally fractured formations was studied by solving intermittent and continuous hydraulic fracturing equations separately by using a combination of X-FEM and phase field model.[69]

V. INFLUENCING FACTORS OF SHALE IMBIBITION

Shale is generally hard, with a dense internal structure, phyllotactic or lamellar lamination, and a large amount of organic matter, which is different from conventional reservoirs.[70] Most of the shale gas is stored in the micro-nano-pores and micro-fractures of the shale matrix, and the fracturing fluid undergoes seepage and drives out the shale gas after hydraulic fracturing. Understanding the influencing factors of shale seepage can help gain insight into the seepage phenomenon, which can be applied to improve the efficiency of shale gas extraction. In the following, the influencing factors of shale seepage are discussed in terms of both shale properties and fluid properties.

A. Shale properties

A shale pore structure is characterized by ultra-dense and extra-low permeability, and the pore scale spans a wide range, which is generally described by porosity. Shale porosity is generally in the range of 2%–4%,[71] and the initial properties of the rock, such as mineral composition, initial water saturation, temperature, and pressure, can have an effect on the percolation process.

Pore type affects the percolation process by determining the permeability of the shale. In strongly hydrophilic cores, the greater the permeability, the faster the percolation rate, and the higher the ultimate percolation recovery. Pore types of marine and terrestrial shales can be divided into organic and inorganic.[72–74] Spontaneous percolation oil drive efficiency is closely related to the core porosity permeability, and there is a permeability value that makes the oil drive efficiency optimal.[73] The influencing factors of the seepage characteristics are more complex, taking the shale of Sec. VII of the Yanchang Formation in the Ordos Basin as an example, as shown in Fig. 12.[75] For cores with little difference in porosity, the lower the organic carbon content, the better the fracturing fluid percolation effect.[76]

Wettability refers to the ability or tendency of liquid molecules to spread on the rock surface, and the organic matter contained in shale reservoirs can change the wettability of shale, thus causing the shale to exhibit a more complex percolation phenomenon. The main factors affecting the wettability of rocks are surface roughness, fluid properties, mineral composition, organic matter, reservoir properties, and gas content.[74] Shale pore space is generally classified into oil-wet, water-wet, and complex-wet spaces according to the wetness of the rock.[77] In the order of permeability, the cores are strong water-wet cores, medium water-wet cores, and weak water-wet cores.[76] Sun *et al.* found that the recovery rate of a surfactant in hydrophilic low-permeability cores was higher than that in oleophilic low-permeability cores at high temperatures,[30] but the improvement in percolation in oleophilic cores was more pronounced for the active agent.[27] The effect of surfactants on the recovery of hydrophilic

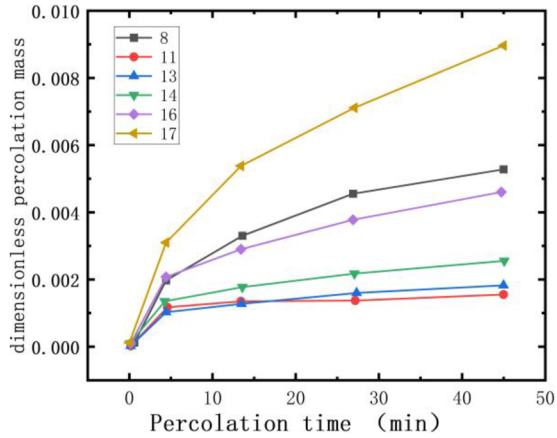

FIG. 12. Spontaneous osmosis pre-curve.

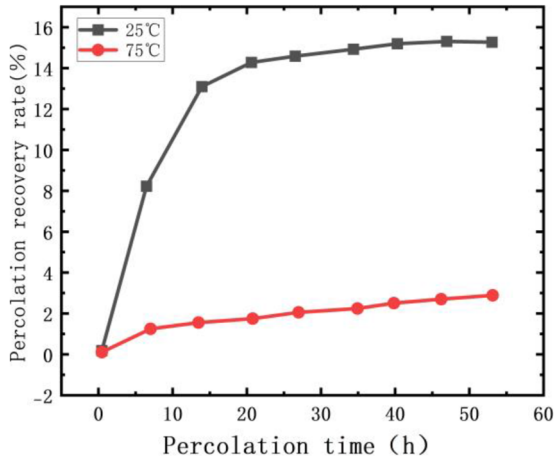

FIG. 13. Effect of temperature on shale percolation.

low-permeability cores at high temperatures was higher than that of hydrophilic low-permeability cores. Wei *et al.*,[78] Cai and Que proposed that wettability has a significant effect on the distribution of two-phase fluids[79] and gave a prediction method for the effect of repulsion efficiency under different wetting conditions. It was found that hydrophobic walls would promote the seepage rate and hydrophilic walls would slow down the seepage rate.

The initial water saturation refers to the ratio of the volume of water in the rock to the volume of the rock pore space before seepage occurs. The initial water saturation of shale increases with the increase in the rock's structural complexity.[80] This is because as the complexity increases, the particle diameter decreases, so the mud content increases; thus, capillaries contain more water, and the water saturation is greater. Rocks that contain high water saturation generally have a high resistivity, Wang *et al.* mentioned that the reason for the low resistivity of the shale of the Wufeng–Longmaxi Formation in the Sichuan Basin is having a high organic matter content,[81] and the key factors affecting the beginning water saturation are organic matter, clay minerals, and their bound water pore volume. It is generally believed that the increase in temperature will promote the effect of percolation and that the total volume and rate of percolation will increase when the temperature increases.[44] The total amount and rate of seepage in individual cores decrease with increasing temperature because the interfacial tension of the fluid decreases at high temperatures, which is the main force driving the seepage, as shown in Fig. 13.[76] By comparing the effect of 0.1, 5, and 10 MPa pressure on seepage, it is found that the seepage rate after pressurization is larger than that before pressurization and the total seepage also increases with the increase in pressure, which indicates that the seepage rate and total seepage increase with the increase in pressure in a certain range.[44]

The mineral composition determines the pore type and wettability of the shale to some extent. The transfer and absorption of clay minerals can lead to changes in the pore structure, which in turn leads to differences in percolation effects. Shale mainly contains clay minerals, quartz minerals, calcite, feldspar, and pyrite.[80] The total amount of percolation increases with increasing clay content.[75] The seepage process is generally divided into a clay-dominated zone and capillary-dominated zone, and it is believed that capillary absorption and swelling will take place only after the clay absorption reaches saturation.[82] The effect of clay minerals on seepage is through influencing the initial water saturation of the rock, and the higher the content of total organic carbon (TOC) in the shale, the slower the seepage rate, and the lower the total seepage.[76]

B. Fluid properties

The different stages of fracturing fluid injection into a well during shale gas extraction are pre-fracturing fluid, sand-carrying fluid, and topping fluid. The nature of the fracturing fluid itself affects the percolation process and can be discussed in terms of interfacial tension and fluid composition. Interfacial tension can be understood as the contraction force at the fluid interface, and the mechanism of formation is the R-value equilibrium theory, which is the result of molecular interaction at the interface layer. There are different views on the effect of interfacial tension on the percolation rate. One view is that the reduction in interfacial tension is beneficial to the percolation, and it is found experimentally that the use of active water can enter smaller pores to reduce the interfacial tension, which can increase the oil yield and promote the percolation process.[58,83] Several studies have shown that there is an optimal interfacial tension to maximize the percolation recovery.[84] The optimal interfacial tension is shown in Fig. 14. The other view is that the reduction in interfacial tension is not conducive to percolation. Since the driving force of percolation includes capillary force, when the interfacial tension is reduced, the capillary force is also reduced, which means that the percolation force is reduced, thus slowing down the percolation process.[85,86]

The effect of ion content in the fluid on the percolation process is mainly through changing the permeability and wettability. The main driving forces of fracturing fluid percolation are capillary force and clay osmotic pressure.[80] The use of cationic active agents and salt particle solutions can reduce the permeability because inorganic salt ions form a double electric layer on the rock surface and reduce the water wettability of the rock.[74] The effect of fracturing fluid composition on the percolation process was obtained by an experimental method,[87] and the results showed that the addition of a cationic active agent and 10% KCL solution to the fracturing

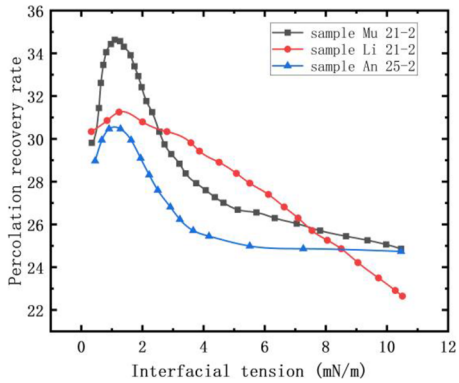

FIG. 14. Variation in percolation recovery with interfacial tension for different cores.

fluid reduced the percolation capacity of shale. The cationic active agent increases the wetting angle of the shale surface, and the 10% KCL solution inhibits the swelling of viscous minerals, resulting in a reduction in seepage capacity. Cations can inhibit the hydration of clay minerals and reduce the percolation rate.[88,89]

VI. CONCLUSIONS AND PROSPECTS

In this study, the progress of shale imbibition research is reviewed in four aspects: imbibition models in shale, progress of imbibition experiments, numerical simulation, and influencing factors of imbibition. The main conclusions from this study are summarized as follows:

1. The LW model yields a linear relationship between the seepage distance and $\sqrt{t}$; the OEO and TEO models developed based on the piston repulsion model can obtain more accurate expressions for the front end of the seepage surface; the factorless time t_D in the scalar model needs to be revised according to the specific seepage situation.
2. The nuclear magnetic technique is concentrated in shale pore distribution characterization, porosity measurement, seepage fluid flow and type analysis, and wettability discrimination; the CT technique is used to find that there are three pore types of marine shale: organic matter pore, clay mineral intergranular pore, and mineral dissolution pore.
3. The combination of the MD method and LBM can obtain the flow pattern in shale nanopores; using numerical simulation techniques such as CFD, it is found that the early flow behavior of shale is determined by the geometry of fractures, and the process of hydraulic fracturing of the formation can be simulated at the same time.
4. The shale pore type changes the percolation process by affecting the permeability; the larger the permeability, the faster the percolation rate. The transfer and absorption of clay minerals will lead to changes in the pore structure, which in turn affects percolation. The percolation process is generally divided into clay-dominated and capillary-dominated zones.

The influencing factors of higher water absorption than oil absorption in the process of spontaneous experiments conducted on standard plunger small cores are complex, and each factor affects each other. The influence of each individual factor on water absorption is unclear and needs to be studied in an extended way. There are few studies on shale powder percolation at home and abroad, and powder experiments can extend the understanding of pore connectivity, so it is necessary to carry out related studies and establish the corresponding normalized recovery model. Wettability is one of the factors controlling the suction swelling caused by capillary suction, and improving the measurement method of the macroscopic contact angle and the contact angle measurement method considering the fluid–solid coupling effect in shale nanopores is a hot direction for research.

Although some experimental results are approximately the same as the field results, the geological mechanisms behind these observations have not been verified. It is mainly due to the various coupled processes occurring in the reservoir that make experimental studies extremely difficult and, to some extent, also due to the variability of mineralogy, which then leads to the inability to fully simulate the real shale reservoir conditions in the experiments. At the same time, the loss of large amounts of fracturing fluid from shale formations during the extraction of shale not only destroys the capacity of the reservoir but also wastes large amounts of repeatable water, putting pressure on areas where water resources are scarce. Therefore, the future research direction is devoted to solving the problems such as the formation mechanism of microfractures and the different percolation lengths of different shales, as well as improving the recovery rate of fracturing fluid and the impact of mining on the water resources in shale reservoirs.

ACKNOWLEDGMENTS

This work was supported by the National Natural Science Foundation of China (Grant No. 12172362), the China National Petroleum Corporation (CNPC) Innovation Found (Grant No. 2021DQ02-0204), and the Youth Innovation Promotion Association of Chinese Academy of Sciences (Grant No. 2023024).

AUTHOR DECLARATIONS

Conflict of Interest

The authors have no conflicts to disclose.

Author Contributions

Mingcan Wang: Writing – original draft (equal). **Weijun Shen**: Supervision (equal). **Tianran Ma**: Supervision (equal). **Zhi Zeng**: Supervision (equal). **Fengchang Yang**: Supervision (equal).

DATA AVAILABILITY

The data that support the findings of this study are available from the corresponding author upon reasonable request.

REFERENCES

[1] W. Shen, X. Li, T. Ma, J. Cai, X. Lu, and S. Zhou, "High-pressure methane adsorption behavior on deep shales: Experiments and modeling," Phys. Fluids **33**, 063103 (2021).

[2] C. Qian, X. Li, Q. Zhang, Y. Li, W. Shen, H. Xing, P. Shu, and Y. C. Y. Huang, "Methane adsorption characteristics under in situ reservoir conditions of the

Wufeng–Longmaxi Shale in southern Sichuan Basin, China: Implications for gas content evaluation," Nat. Resour. Res. **32**, 1111–1133 (2023).
[3]W. Li, H. Zhang, T. Luo, W. Wu, L. Jiang, Z. Zhong, Y. Jiang, Y. Fu, and G. Cai, "Influence of microscopic pore structure of shale reservoirs on shale gas availability in west Yu area," Nat. Gas Geosci. **33**, 873–885 (2022).
[4]W. Shen, L. Zuo, T. Ma, C. Chen, C. Qin, L. Yang, and K. Xie, "Quantitative studies on the characterization and evaluation of adsorbed gas and free gas in deep shale reservoirs," Energy Fuels **37**, 3752–3759 (2023).
[5]M. Jia, L. Zhang, and J. Guo, "Combining a connected-component labeling algorithm with FILTERSIM to simulate continuous discrete fracture networks," Environ. Earth Sci. **76**, 327 (2017).
[6]W. Shen, X. Li, X. Lu, W. Guo, S. Zhou, and Y. Wan, "Experimental study and isotherm models of water vapor adsorption in shale rocks," J. Nat. Gas Sci. Eng. **52**, 484–491 (2018).
[7]C. Qian, X. Li, Q. Zhang, W. Shen, W. Guo, W. Lin, L. Han, Y. Cui, Y. Huang, X. Pei, and Z. Yu, "Reservoir characteristics of different shale lithofacies and their effects on the gas content of Wufeng-Longmaxi Formation, southern Sichuan Basin, China," Geoenergy Sci. Eng. **225**, 211701 (2023).
[8]L. Richard, "The time law of capillary growth," Ophthalmologica **23**, 15–22 (1918).
[9]E. Washburn, "The dynamics of capillary flow," Phys. Rev. D **17**, 273–283 (1921).
[10]K. Li and R. Horne, "Characterization of spontaneous water imbibition into gas-saturated rocks," SPE J. **6**, 375–384 (2001).
[11]S. Supple and N. Quirke, "Molecular dynamics of transient oil flows in nanopores I: Imbibition speeds for single wall carbon nanotubes," J. Chem. Phys. **121**, 8571 (2004).
[12]Z. Zhang, J. Y. Feng, J. Cai, K. Chen, and Q. Meng, "Percolation driving factors under different boundary conditions," J. Comput. Phys. **38**, 513–520 (2021).
[13]L. Handy, "Determination of effective capillary pressures for porous media from imbibition data," Trans **219**, 75–80 (1960).
[14]D. Standnes, "Experimental study of the impact of boundary conditions on oil recovery by co-current and counter-current spontaneous imbibition," Energy Fuels **18**, 271–282 (2004).
[15]L. Wang, F. Ma, Y. He, and D. Liu, "The prediction of spontaneous oil-water imbibition in composite capillary," Petroleum **8**, 84–91 (2022).
[16]A. Hamraoui and T. Nylander, "Analytical approach for the lucas–Washburn equation," J. Colloid Interface Sci. **250**, 415–421 (2002).
[17]H. Fischer, S. Wo, and N. Morrow, "Modeling the effect of viscosity ratio on spontaneous imbibition," SPE Reserv. Eval. Eng. **11**, 577–589 (2008).
[18]G. Mason, H. Fischer, N. Morrow, and D. Ruth, "Correlation for the effect of fluid viscosities on counter-current spontaneous imbibition," J. Pet. Sci. Eng. **72**, 195–205 (2010).
[19]J. Cai, C. Zhao, L. Tan, and X. Hu, "Fractal analysis of percolation coefficient of porous media in low-permeability reservoirs," Bull. Geol. Sci. Technol. **30**, 54–59 (2011).
[20]G. Xie, "Measurement of adhesion force on the inner wall of capillary bundle rheology model and study of influencing factors," J. Nat. Sci. Heilongjiang Univ. **1**(53–55), 60 (2005).
[21]J. Cai and B. Yu, "Advances in spontaneous percolation in porous media," Adv. Mech. **42**, 735–754 (2012).
[22]Y. Xue, L. Shi, Y. Cao, M. Liu, and C. Xin, "A new numerical simulation model for nonlinear seepage flow. Exploit," Unconv. Oil Gas Resour. **9**, 103–116 (2022).
[23]L. Rapoport and W. Leas, "Properties of linear waterfloods," J. Pet. Technol. **5**, 139–148 (1953).
[24]S. Ma, N. Morrow, and X. Zhang, "Generalized scaling of spontaneous imbibition data for strongly water-wet systems," J. Pet. Sci. Eng. **18**, 165–178 (1997).
[25]K. Li and R. Horne, "An analytical scaling method for spontaneous imbibition in gas/water/rock systems," SPE J. **9**, 322–329 (2004).
[26]L. Yang, N. Dou, X. Lu, X. Zhang, and X. Hen, "Advances in understanding imbibition characteristics of shale using an NMR technique: A comparative study of marine and continental shale," J. Geophys. Eng. **15**, 1363–1375 (2018).
[27]Y. Sun, "A review of the application of nuclear magnetic resonance in the evaluation of shale reservoir parameters," Adv. Geophys. **08**, 1–18 (2022).
[28]X. Cheng, H. Liu, W. Xiong, S. Gao, and Z. Hu, "Experimental study on spontaneous percolation in low-permeability sand and conglomerate reservoirs in Xinjiang," Sci. Tech. Eng. **13**, 7793–7797 (2013).
[29]R. Wang, C. Yang, H. Ru, P. Wang, and Y. Yang, "Comparison of errors between shale and coal in volumetric isothermal adsorption experiments," Unconv. Oil Gas. **8**(43–48), 57 (2021).
[30]L. Sun, W. Pu, J. Xin, and Y. Wu, "Effect of surfactants on high-temperature percolation in low-permeability cores," J. China Univ. Pet., Ed. Nat. Sci. **36**, 5 (2012).
[31]D. Lu, J. Zhang, Y. Zhang, Y. Chi, and C. Zhao, "Experimental study on the enhancement of shale gas recovery by CO_2 injection," J. Dalian Univ. Technol. **61**, 464–470 (2021).
[32]S. Xi, W. Mo, X. Liu, L. Zhang, and J. Li, "Exploration potential of shale gas in the Ulalik formation of the ordos system on the western margin of the Ordos Basin: The zhongping 1 well as an example," Nat. Gas Geosci. **32**, 1235–1246 (2021).
[33]B. Shi, B. Xia, YX. Lin, and J. Xu, "CT imaging and mechanism of hydrated fracture development in hard and brittle mud shale," Acta Pet. Sin. **33**, 137–142 (2012).
[34]Q. Chen, Y. Kang, L. You, Y. Yu, and H. Liu, "Shale micropore structure and its effect on gas transfer mode," Nat. Gas Geosci. **24**, 1298–1304 (2013).
[35]H. Yang, X. Niu, L. Xu, S. Feng, and Y. You, "Exploration potential of shale oil in Change 7 member, upper triassic Yanchang formation, Ordos Basin, NW, China," Pet. Explor. Dev. **43**, 560–569 (2016).
[36]J. Yang, "Analysis of the percolation mechanism of porous media and its influencing factors," Yunnan Chem. Technol. **47**, 138–140 (2020).
[37]D. Schechter, D. Zhou, and F. Orr, "Capillary imbibition and gravity segregation in low IFT system," SPE **6**, 22594 (1991).
[38]M. Meng, H. Ge, W. Ji, W. Shen, Y. Su, and H. Ai, "Monitor the process of shale spontaneous imbibition in co-current and countercurrent displacing gas by using low field nuclear magnetic resonance method," Nat. Gas Sci. Eng. **27**, 336–345 (2015).
[39]B. Li, S. Deng, Y. Liu, S. Cao, and D. Jin, "Determination of movable fluid saturation in the Gulong shale oil reservoir in the Songliao Basin," Pet. Geol. Oilfield Dev. Daqing. **41**, 130–138 (2022).
[40]C. Li, B. Shen, L. Lu, Q. Jiang, A. Pan, J. Tao, and J. Ding, "Characterization of shale pore structure in the Shahezi Formation of the Songliao Basin—Based on low-field nuclear magnetic resonance technique," Oil Gas Res. Eva. Dev. **12**, 468–476 (2022).
[41]Q. Sun, W. Wang, Y. Su, J. Xu, and X. Guo, "Characteristics of microscopic pore crude oil mobilization during percolation of fracturing fluid in shale reservoirs," J. Cent. South Univ. (Engl. Ed.). **53**, 3311–3322 (2022).
[42]W. Pu, J. Chang, B. Zou, R. Liu, and D. Du, "Application of nuclear magnetic resonance measurement technique to measure thick oil-water relative permeability curves," Oilfield Chem. **11**, 1–8 (2022).
[43]Y. Wan, X. Cao, H. Liu, Q. Ma, and Z. Bai, "Self-absorption characteristics of shales in the Luchaogou formation of the Santang lake Basin," Xinjiang Pet. Geol. **41**, 666–676 (2020).
[44]Y. Zhu and Z. Li, "Seepage law and dynamic distribution of seepage in the Longmaxi Formation shale of Pengshui area," J. Comput. Phys. **38**, 555–564 (2021).
[45]H. Chen, F. Guan, J. Zhang, H. Hu, and S. Lu, "A new method for calculating shale gas adsorption volume under high pressure," Oil Gas Geol **26**, 87–93 (2019).
[46]C. Yue, S. Li, L. Li, and H. Wen, "Study on isothermal desorption characteristics of shale gas," Geosci. J. Grad. Sch., China Univ. Geosci. **31**, 150–157 (2017).
[47]D. Yang, Y. Kang, J. Wu, L. You, and X. Song, "Experimental study on the mechanism of high-temperature thermally excited percolation in organic-rich shale," J. Xi'an Shiyou Univ., Nat. Sci. Ed. **37**, 55–60 (2022).
[48]LH. Pan, H. Wang, J. He, Y. Tian, and X. Liao, "Experimental study on the effect of shale hydration on proppant embedding," Sci. Tech. Eng. **22**, 5228–5235 (2022).
[49]W. Han, C. Gao, and X. Han, "Application of nuclear magnetic resonance and micro- and nano-CT technology in the study of tight reservoirs—Example of long section 7 in Ordos basin," Fault-Block Oil Gas Field **22**, 62–66 (2015).
[50]J. Wu, H. Fan, J. Zhang, H. Hu, and S. Wan, "Experimental study on stress sensitivity of artificial fracture in shale - an example of Longmaxi Formation shale in south Sichuan area," Nat. Gas Ind. **42**, 71–81 (2022).

[51]L. Mao, Y. Bi, H. Liu, J. Chen, and J. Wang, "Research progress of rock internal deformation field measurement method based on CT imaging and digital body image correlation method," Sci. Bull. **11**, 1–19 (2022).
[52]S. Supple and N. Quirke, "Molecular dynamics of transient oil flows in nanopores. II. Density profiles and molecular structure for decane in carbon nanotubes," J. Chem. Phys. **122**, 104706 (2005).
[53]S. Wang, F. Javadpour, and Q. Feng, "Molecular dynamics simulations of oil transport through inorganic nanopores in shale," Fuel **171**, 74–86 (2016).
[54]S. Zhang, "Molecular dynamics simulation of shale oil fractionation characteristics in Dongying Depression," Oil Gas Geol **28**, 74–80 (2021).
[55]T. Huang, L. Cheng, R. Cao, P. Wang, and Z. Jia, "Molecular dynamics simulation of the transport characteristics of shale oil on inorganic mineral surfaces," J. Xi'an Shiyou Univ., Nat. Sci. Ed. **37**, 42–48 (2022).
[56]X. Hong, H. Xu, F. Cui, H. Yu, Y. Wu, H. Wu, and F. Wang, "Application of molecular simulation in unconventional oil and gas development," Chin. J. Comput. Mech. **38**, 313–320 (2021).
[57]Y. Hu, C. Zhao, J. Zhao, J. Wang, Q. Zhao, J. Gao, D. Fu, and C. Fu, "Mechanisms of fracturing fluid spontaneous imbibition behavior in shale reservoir: A review," J. Nat. Gas Sci. Eng. **82**, 103498 (2020).
[58]C. Li, H. Singh, and J. Cai, "Spontaneous imbibition in shale: A review of recent advances," Capillarity **2**, 17–32 (2019).
[59]C. Aidun and J. Clausen, "Lattice-Boltzmann method for complex flows," Annu. Rev. Fluid Mech. **42**, 439–472 (2010).
[60]X. Shan and H. Chen, "Lattice Boltzmann model for simulating flows with multiple phases and components," Phys. Rev. E **47**, 1815–1819 (1993).
[61]J. Zheng, Y. Ju, and M. Wang, "Pore-scale modeling of spontaneous imbibition behavior in a complex shale porous structure by pseudopotential lattice Boltzmann method," J. Geophys. Res. **123**, 9586–9600, https://doi.org/10.1029/2018jb016430 (2018).
[62]H. Wang, Y. Su, and W. Wang, "Improved lattice Boltzmann method to simulate liquid flow in nanoporous media: Coupling molecular dynamics simulations and theoretical model," Adv. Water Resour. **165**, 104239 (2022).
[63]K. T. Jiao, D. Han, D. Wang, Y. Chen, and J. Li, "Investigation of thermal-hydro-mechanical coupled fracture propagation considering rock damage," Comput. Geosci. **26**, 1167–1187 (2022).
[64]W. Zhou, X. Yang, and X. Liu, "Multiscale modeling of gas flow behaviors in nanoporous shale matrix considering multiple transport mechanisms," Phys. Rev. E **105**, 055308 (2022).
[65]X. Qiu, G. Zhong, X. Li, M. Chen, and W. Ling, "CFD simulation study of flow characteristics of horizontal shale gas wells with different well slopes," Oil Gas Res. Eva. Dev. **11**, 1–10 (2022).
[66]J. Samuel and G. Andrea, "Numerical simulation of shale gas flow in three-dimensional fractured porous media," Uncon. Oil Gas **16**, 90–112 (2016).
[67]T. Jiang, H. Wang, J. Wei, G. Zhong, and Y. Zhao, "Migration law and influence of proppant in segmented multicluster fracturing wellbore of deep shale horizontal well," Geofluids 1–16 (2022).
[68]Y. Yang, L. Xie, B. He, and P. Zhao, "Numerical study on the use of alternating injection hydraulic fracturing technology to optimize the interaction between hydraulic fracture and natural fracture," Front. Earth Sci. **10**, 873715 (2022).
[69]J. Zhang, H. Yu, W. Xu, C. Lu, and M. Micheal, "A hybrid numerical approach for hydraulic fracturing in a naturally fractured formation combining the XFEM and phase-field model," Eng. Fract. Mech. **271**, 108621 (2022).
[70]W. Shen, F. Song, X. Hu, G. Zhu, and W. Zhu, "Experimental study on flow characteristics of gas transport in micro-and nanoscale pores," Sci. Rep. **9**, 10196 (2019).
[71]J. He, Y. Xie, J. Liu, and L. He, "Geological characteristics of deep Longmaxi Formation shale reservoirs in the southwest margin of the Sichuan Basin: An example from the Leibo area of the Zhaotong shale gas demonstration area," Nat. Gas Geosci. (published online, 2023).
[72]D. Han, Y . Peng, and S. Guo, "Percolation pattern of surfactant on water-wet sandstone and its effect on recovery rate," J. China Univ. Pet., Ed. Nat. Sci. **33**, 142–147 (2009).
[73]J. Zhong, X. Yang, Y. Chen, H. Tang, and D. Lu, "A new method for natural percolation experiments in low-permeability cores," Petrochem. Ind. Appl. **32**, 61–65 (2013).
[74]T. Cao, M. Deng, J. Xiao, H. Liu, and A. Pan, "Characteristics of sea-land transition phase shale reservoirs and gas-bearing reservoir mechanism based on comparison with marine shale reservoirs," Nat. Gas Geosci. **11**, 1–22 (2022).
[75]X. Zhou, D. Chen, Y. Xia, J. Zeng, and J. Qiao, "Spontaneous seepage characteristics and influencing factors of shale oil reservoirs in longdong area, Ordos Basin, Section 7," Earth Sci **47**, 3045–3055 (2022).
[76]L. Yan, "Analysis of factors influencing percolation of fracturing fluid in shale gas reservoirs," Liaoning Chem. Ind. **51**, 606–608 (2022).
[77]S. He, "Revisiting the concept of wettability in dense rocks rich in organic matter: Application to formation injury-water lock," Nat. Gas Exp. Dev. **43**, 47 (2020).
[78]H. Wei, R. Hu, Z. Liao, and Y. Chen, "Influence of wettability on the efficiency of two-phase seepage repulsion in pore media," J. Mech. **53**, 1008–1017 (2021).
[79]P. Cai and Y. Que, "Numerical study of two-phase seepage characteristics of porous media considering wall wettability," Eng. J. Wuhan Univ. **09**, 1–9 (2022).
[80]J. Wang, M. Feng, W. Yan, and S. Liu, "Influencing factors and calculation methods of water saturation in shale gas reservoirs—Example of the Wufeng formation-Longmaxi formation in the Jiaoshiba block," Nat. Gas Tech. Eco. **14**, 21–28 (2020).
[81]L. Wang, S. Li, X. Liu, Y. Hou, and H. Zhou, "Evaluation of water saturation logging in low resistance shales of the Wufeng-Longmaxi formation in the Sichuan Basin," Sci. Tech. Eng. **22**, 6456–6462 (2022).
[82]A. Zolfaghari, H. Dehghanpour, and J. Holyk, "Water sorption behaviour of gas shales: I. Role of clays," Int. J. Coal Geol. **179**, 130–138 (2017).
[83]Z. Wu, Z. Gao, S. Ma, J. Zhao, and J. Shi, "A preliminary investigation of oil percolation and oil repelling phenomenon in the long 7 section shale oil of Ordos Basin," Nat. Gas Geosci. **32**, 1874–1879 (2021).
[84]Q. Liu, J. Zhang, H. Shi, X. Li, and B. Guan, "Effectiveness and mechanism of recovery enhancement by surfactant systems with different interfacial properties," Oilfield Chem. **09**, 1–11 (2022).
[85]J. Chen, H. Tang, X. Xu, L. Lu, and H. Liao, "Analysis of the effect of surface activator on percolation and oil repelling effect of low permeability fractured sandstone reservoir," Offshore Oil **01**, 51–55 (2008).
[86]X. Liu, L. Yan, Y. Zhang, and X. Fan, "Analysis of factors influencing spontaneous percolation in dense sandstone reservoirs," Yunnan Chem. Technol. **48**(55–57), 71 (2021).
[87]F. Zhou and W. Chen, "Experimental study of percolation in low permeability cores," Compl. Hydroc. Reserv. **2**, 54–56 (2009).
[88]J. Xiong, S. Chen, L. Liang, Y. Xiao, and L. Tan, "Percolation characteristics of Longmaxi formation shale and its influencing factors," J. Guilin Univ. Technol. **40**, 688–694 (2020).
[89]Z. Li, Z. Lei, W. Shen, D. A. Martyushev, and X. Hu, "A comprehensive review of the oil flow mechanism and numerical simulations in shale oil reservoirs," Energies **16**, 3516 (2023).